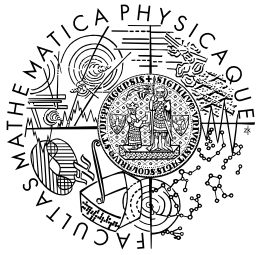

FACULTY
OF MATHEMATICS
AND PHYSICS
Charles University

BACHELOR THESIS

Jindřich Dušek

$1/f$ noise in an algebraic model of molecular vibrations

Institute of Particle and Nuclear Physics

Supervisor of the bachelor thesis: Mgr. Pavel Stránský, Ph.D.
Study programme: Physics
Study branch: Physics

Prague 2021

I declare that I carried out this bachelor thesis independently, and only with the cited sources, literature and other professional sources. It has not been used to obtain another or the same degree.

I understand that my work relates to the rights and obligations under the Act No. 121/2000 Sb., the Copyright Act, as amended, in particular the fact that the Charles University has the right to conclude a license agreement on the use of this work as a school work pursuant to Section 60 subsection 1 of the Copyright Act.

In ..... date ....

Author's signature

I wish to thank my supervisor Pavel Stránský for his sensible advice and patience. Consultations with you helped to elucidate concepts I had known little about, as well as concepts I had considered familiar. I also thank my mother Markéta and my aunt Petra for their kind support.

Title: $1/f$ noise in an algebraic model of molecular vibrations

Author: Jindřich Dušek

Department: Institute of Particle and Nuclear Physics

Supervisor: Mgr. Pavel Stránský, Ph.D., Institute of Particle and Nuclear Physics

Abstract: $1/f$ noise is commonly observed in many complex systems. In quantum systems it can serve as a chaos indicator without any reference to the properties of concrete RMT ensembles. We use the $1/f$ noise analysis to study a perturbed vibron model, which is a finite quantum system previously applied for description of linear molecules or a Bose-Einstein condensate. The results are in a partial agreement with the classical limit of our model with discrepancies observed for the integrable limit of the model. Such discrepancies are yet to be explained. We also suggest some improvements to our procedure, namely studying systems with a greater dimension, combining multiple systems with similar dimensions, or changing the length of the analysed time series. Lastly, we mention an inherent restriction of our procedure: the need for manual analysis of each system with particular parameters. This limitation restricts the usability of the $1/f$ noise analysis and it remains to be seen, whether it can be overcome.

Keywords: $1/f$ noise, quantum chaos, molecular vibration, many-body system

Contents

Introduction

Mathematical concepts such as numbers usually have a lot of depth to them. They are even infinite in some sense and theorems we discover using mathematical methods are universally valid. That doesn't mean, however, that mathematics is universally and infinitely applicable as a solution to real life problems. There are always limits to the accuracy with which we can measure and those limits affect the accuracy of our predictions disproportionately. Moreover, the language of mathematical theorems is inherently different from human languages and as a result of that mathematics rarely answers the questions people are truly asking[1].

Classical chaos theory operates with those restrictions in mind. It is a field of classical mechanics that describes systems where even the slightest changes of initial conditions result in unpredictable alterations of the resulting motion. So even though the physical laws which determine the system completely are known, it is impossible to describe how the motion will turn out in practice. We must therefore accept our restraints and give up on trying to know everything. Even so, chaos theory can still provide valuable insights.

The chaos in chaos theory arises due to measurement errors present in all measurements. But errors and uncertainties can be reduced, for instance by improving our measuring instruments or choosing better measuring methods. If we regard our uncertainties as "classical uncertainties", it is in theory possible to reduce our measurement error ad absurdum. This is, however, not the case in *quantum mechanics*.

In quantum theory the concept of measurement uncertainties is fundamentally imbued in our description of reality (i. e. in *quantum states*). Most importantly, Heisenberg's uncertainty principle forbids the measurement error of physical quantities to vanish even for the most accurate of measurements. As a result of this, the notion of "trajectory" or "immediate position" is alien to quantum mechanics; all quantum states are described in terms of probabilities.

The definition of quantum chaos is still not completely firm – some suggest talking about quantum chaology instead of quantum chaos [2]. It is most often defined via *spectral correlations*. We examine the permissible energies of a bound quantum state and use their distribution to determine if a system is chaotic. Usually, various statistical methods are used to analyse the energy spectrum at hand. In this work we shall focus on analysing the so-called $1/f$ *noise* as described in [3] and [4].

$1/f$ noise is not an isolated feature of quantum-mechanical systems. In fact, it has been observed in music, shapes of mountains or in human cognition to name a few examples [5, 6]. In [7, 8] it has been suggested that the $1/f$ is a general sign of complex systems, which makes this indicator interesting. To find $1/f$ in quantum mechanics we in short treat the energy spectrum as a time series, use discrete Fourier analysis to obtain its frequencies and look at their distribution. According to theory, if the frequencies behave as $1/f$, the system is chaotic, if as $1/f^2$, it isn't.

Our model of choice is the vibron model based on the $u(3)$ algebra, which is

[1] For an example of a grave misunderstanding between man and the personification of mathematical exactness see the legend of the golem of Prague [1].

described in [9]. We have chosen this model for its relative simplicity and because it has already been examined in its classical limit in [10]. We can thus compare our results with the classical limit and test, whether the $1/f$ noise method is useful in determining the chaoticity of the system.

1. Classical versus Quantum chaos

The aim of this chapter is to briefly describe the theoretical underpinnings behind our explanation of quantum chaos and how it differs from the conventional[1] classical chaos. While in classical mechanics, *chaotic* systems can be relatively easily distinguished from non-chaotic or *integrable* systems, this distinction is much more blurry in quantum mechanics. Thus a brief overview of classical chaos shall show the ways in which classical and quantum chaos differ, but it shall also prove useful for one way of defining quantum chaos is through *classical correspondence*.

1.1 Classical systems

When we, from a physical point of view, try to describe the real world, we always implicitly ask ourselves the following questions:

1. What description are we using to symbolise real world objects (i. e. the observed phenomena)?

2. What description are we using to illustrate their interactions (i. e. their temporal evolution)?

In classical non-relativistic mechanics we interpret our world[2] as (some section of) $\mathbb{R}^3$. As the only means of describing real world objects we use *point masses*[3] of negligible size, which represent matter. Real world objects can be regarded either as a single point mass, as a collection of certain point masses, or as a continuum of point masses.

A single point is in each instant determined by its mass m and 6 coordinates q_i and p_i $(i = 1, 2, 3)$, where q_i determine the position of the point and p_i its momentum (which can be used to calculate its velocity). A *classical state* is the configuration of a system in a given instant. If we disregard the case of continua, we only need to describe a configuration of N point masses. A classical state can thus be represented as two $3N$-dimensional vectors $\vec{q}$ and $\vec{p}$, where coordinates and momenta of all involved particles are stored.

To describe the interactions of particles with each other, we must first remember we are talking about our system in the framework of classical mechanics. Therefore, the evolution of our system has to be in accordance with *Newton's laws of motion* or, in a more abstracted form, with the *Hamiltonian formalism*. Usually, Hamiltonian formalism is preferred, its summary is presented in [11], but roughly speaking, a single function $H(\vec{q}, \vec{p})$ called the *Hamiltonian* can be used to determine the evolution of our system (we restrict ourselves to time-independent Hamiltonians).

To identify a system we must also find its Hamiltonian. Together with $\vec{p}$ and $\vec{q}$ and possible boundary conditions, it determines a physical system completely. In summary, a physical model used for the description of the real world consists of:

[1] We consider classical chaos more conventional as it has been studied for a longer period of time and more thoroughly. Moreover, chaotic systems such as a double pendulum feel more familiar than quantum systems.

[2] In some sense, physical space is also an observed phenomenon.

[3] Also called points or particles.

1. a theoretical framework (in this case classical mechanics),
2. a set of physical objects—the state (in this case $\vec{p}$ and $\vec{q}$),
3. parameters that determine the interactions in this theoretical framework (in this case the form of Hamiltonian and boundary conditions).

1.1.1 Classical integrability

We distinguish two regularity classes of systems: integrable and chaotic. In the integrable case, there are as many independent integrals of motion—quantities that are conserved along the trajectory in phase space—as there are degrees of freedom. In such a case, the system is *solvable*, i. e. trajectories of particles can be explicitly written in terms of analytical functions.

In the chaotic case, the number of independent integrals of motion is lower than the number of degrees of freedom and the system is not solvable. We may also distinguish chaotic states by observing the *phase space*, which is a space of all possible values of $\vec{p}$ and $\vec{q}$. It is the space of all possible states of a system; in the case of N free particles it can be thought of simply as $\mathbb{R}^{6N}$.

For simplicity, let us consider a classical model consisting of a single free particle. Then, the realised state of our system in each time is represented by a point in a 6D phase space. However, no measurement is without errors. Therefore, a point in a phase space is only an idealisation. If we want our description to include errors, we must introduce a small volume V in phase space. This volume represents all possible configurations for our described particle—the real state lies somewhere within V, but we don't know where (see fig. 1.1).

A characteristic of chaoticity in classical mechanics is *sensitivity to initial conditions*, namely that initially close points on phase space drift apart rapidly. When observing a diagram of the phase space, this corresponds to an exponential "sprawl" of the initial volume V. Let us emphasize that thanks to *Liouville's theorem*, the volume V is conserved in time for non-dissipative systems. By chaotic sprawl we mean an erratic deformation of the volume V in such a way that initially close points become distant. This behaviour is representative of chaotic systems: it was the phenomenological motivation for studying chaos and it can be measured to determine the degree of chaoticity. An example of chaotic and nonchaotic evolution of a point (volume) P on phase space can be seen in fig. 1.1.

1.2 Quantum systems

For certain physical systems, the theoretical framework of classical mechanics is not enough and we achieve better results by utilising *quantum mechanics*. In this framework, *quantum states* are described by vectors $|\psi\rangle$, $|\phi\rangle$ or their covectors $\langle\psi|$, $\langle\phi|$. If the scalar product $\langle\phi|\psi\rangle$ exists, its square represents the likelihood that the state $|\psi\rangle$ is mistaken for $|\phi\rangle$. To ensure that $\langle\phi|\psi\rangle$ exists, we choose state vectors to be elements of some Hilbert space[4] $\mathcal{H}$.

[4]More generally, the concept of rigged Hilbert space (the Gelfand triplet) is used to enable us to work with a wider range of states while preserving the valuable concept of a scalar product.

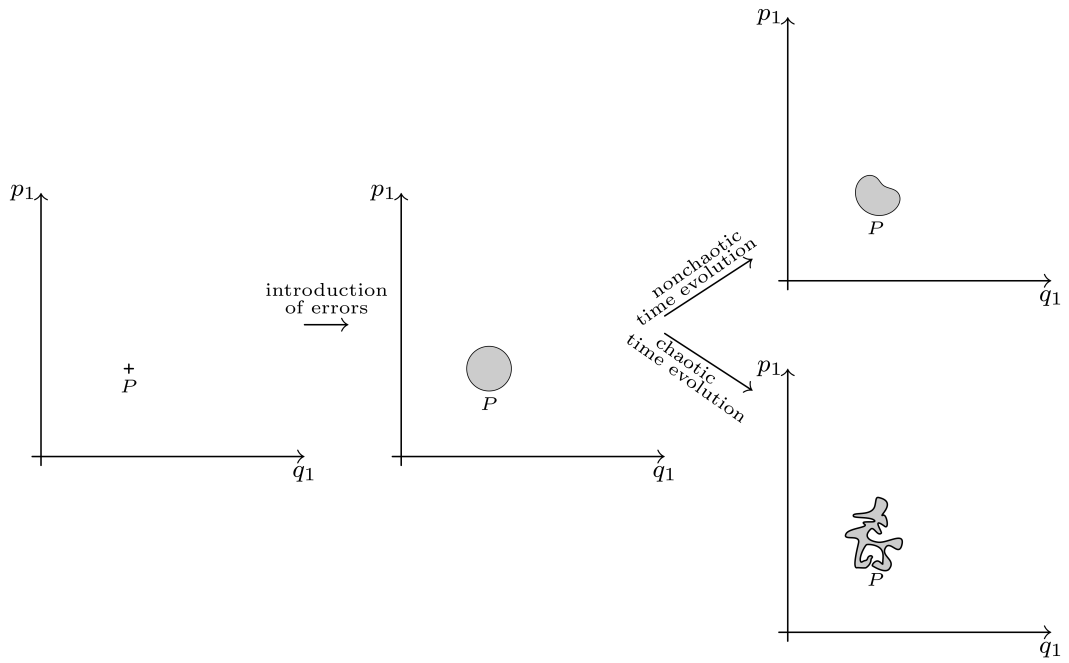

Figure 1.1: Ilustration of chaotic and nonchaotic evolution in a classical phase space. A 2D subspace of the whole phase space is shown.

We shall not discuss how information about observable quantities is encoded in quantum states. For such a discussion along with a more complete overview of quantum mechanics consult [12]. The important thing is that the state vector $|\psi\rangle$ indeed contains all available information about a given configuration of a quantum system just like vectors $\vec{p}$ and $\vec{q}$ in classical mechanics.

The evolution of a quantum system is described by the *Schrödinger equation*. Its concrete form is determined by the Hamiltonian operator $\hat{H}$. It is a hermitean operator that corresponds to the classical Hamiltonian.

1.2.1 Quantum integrability

As in the classical case, we define two regularity classes of quantum system: integrable and chaotic. A quantum state with d degrees of freedom is said to be integrable, if each eigenstate can be uniquely labeled by d quantum numbers, where the quantum numbers correspond to integrals of motion. For a chaotic system this is not possible.

The effects of (non)integrability on quantum systems are however more difficult to pinpoint than in classical mechanics. For instance, while in classical mechanics we can observe the phase space and understand it relatively easily with the help of the so-called Poincaré sections, this is impossible in quantum mechanics[5]. Furthermore, the evolution of quantum states is unitary, which means that $\langle\phi(t)|\psi(t)\rangle$ is constant for each time t and every state $|\psi\rangle$ or $|\phi\rangle$. This means that individual quantum states don't change their distance, they don't drift apart in the same sense as classical states do.

As it is impractical to look at individual states directly and compare them, we

[5]There is no direct quantum analogy to Poincaré sections, although a similar tool called the Peres lattices exists [13].

instead examine the Hamiltonian—it determines the evolution of the system. To do so, the most convenient way is to investigate its eigenenergies: thanks to the *spectral theorem*, we know that a hermitean operator is completely determined by its eigenvalues, therefore the set of all eigenergies—the *spectrum*, becomes the most fundamental object of our study.

1.2.2 Spectral correlations

When we analyse the spectrum, we look for *correlations*, i. e. statistical relationships between different energies. In the case of integrable quantum systems, there is again a formula for each eigenenergy in terms of quantum numbers—integrals of motion. Due to this, there is no statistical relationship between different eigenlevels, the spectrum is uncorrelated.

On the other hand there are completely chaotic spectra. In such spectra there are no integrals of motion (besides energy). We have to diagonalise the Hamiltonian to find its eigenenergies and from this process, correlations between energies are introduced. In completely chaotic systems, there are correlations on every scale (we speak of long-, short- or mid-range correlations). No formula can be found to describe individual eigenlevels, as there is a strong relationship between different energies.

As an example of an integrable system we point to the 2D quantum linear harmonic oscillator. Each eigenlevel can be calculated using quantum numbers and the spectrum is therefore uncorrelated. One can understand the correlations of various levels on an example of the price of a popular stock on a stock market. The price in a given instant is highly correlated with its recent prices as trading algorithms try to maximise profits and trade rapidly. Mid-range correlations are introduced as traders react to recent news about the company and long-range correlations can be related to the changing intrinsic value of the stock. Furthemore not only are future prices correlated with historical prices due to causality, but current prices are correlated with future prices as investors buy or sell stocks depending on their expected value.

A quantitative link between spectral correlations and integrability is the *Bohigas-Giannoni-Schmit* conjecture[6] [16]. It states that systems with chaotic classical analogues have spectral correlations in accordance with the *random matrix theory*[7] (RMT). I. e. the Hamiltonian of said system has the same spectral correlations as a random matrix taken from an ensemble of random matrices with a certain probability distribution. The random matrix theory thus serves as a vehicle for making meaningful theoretical predictions about quantum systems and their chaoticity.

[6]This conjecture has not been proven yet, however it is supported by a large amount of numerical studies, for instance the Hydrogen atom in a magnetic field [14] or the hyperbola billiard [15].

[7]For a comprehensive overview of RMT see [17].

2. $1/f$ noise

Complex physical systems from various scientific areas tend to have one thing in common: $1/f$ noise (or pink noise). That is if, in a complex system, we observe phenomena happening with various frequencies, the distribution of said frequencies usually behaves as $1/f$ noise. Various occurences of $1/f$ noise have been studied [5, 6] and there is a consensus that the appearance of $1/f$ noise is not merely a coincidence, but rather a feature of complex systems [7, 8].

Recently, $1/f$ noise has also been shown to occur in chaotic quantum spectra, while integrable spectra have been shown to display $1/f^2$ noise. We will outline how the $1/f^\alpha$ noise can be observed and proceed to use it as an indicator of quantum chaos. As we have discussed in the previous chapter, the distinction between quantum integrability and chaos is still unclear. Having another chaos indicator can thus help with describing quantum chaotic systems and defining the term quantum chaos.

2.1 Unfolding

If we look at the spectra of different Hamiltonians, we want their spectral characteristics to be comparable. For instance, if we have Hamiltonians $\hat{H}_1$ and $\hat{H}_2 = \hat{H}_1 + \alpha$, where α is a constant, their spectral characteristics should be identical, as Hamiltonians represent energy of the observed system and this energy is determined uniquely up to a constant. We should therefore "normalise" our spectra before we study them further. This procedure is called *unfolding*.

To explain unfolding, we proceed as in [18]. Firstly we define the *level density* $\rho(E)$ as

$$\rho(E) = \sum_i \delta(E - E_i)\,, \tag{2.1}$$

where we sum over all energies i and δ is the Dirac delta function. This level density can be decomposed into two parts:

$$\rho(E) = \tilde{\rho}(E) + \overline{\rho}(E)\,, \tag{2.2}$$

where $\tilde{\rho}$ is the *oscillatory* part and $\overline{\rho}$ is the *smooth* part. The smooth part represents the average density of levels around E. The oscillatory part represents deviations from the average, only it contains information about correlations. When analysing correlations, we want to trivialise the smooth part, as it is not important, and focus on the oscillatory part.

Unfolding thus consists of transforming eigenenergies from E_i to dimensionless e_i, such that $\overline{\rho}(e) = 1$. It can be shown that this transformation can be done using the smooth *cumulative level density* [19, p. 74]. Generally, the cumulative density $\mathcal{N}(E)$ counts the number of levels with energy $\leq E$, it is defined as

$$\mathcal{N}(E) = \int_{-\infty}^{E} \rho(E')\mathrm{d}E'\,. \tag{2.3}$$

Cumulative level density can be similarly decomposed into its smooth and oscillatory part as

$$\mathcal{N}(E) = \overline{\mathcal{N}}(E) + \tilde{\mathcal{N}}(E)\,, \tag{2.4}$$

where

$$\overline{\mathcal{N}}(E) = \int_{-\infty}^{E} \overline{\rho}(E')\mathrm{d}E'\,. \tag{2.5}$$

We can then write

$$e_i = \overline{\mathcal{N}}(E_i)\,. \tag{2.6}$$

The difficult part is to find $\overline{\mathcal{N}}(E_i)$. In the case of systems with semiclassical analogues, we can use the semiclassical Weyl formula [18, eq. (4)] to calculate $\overline{\rho}$ and then use eq. (2.5) to calculate $\overline{\mathcal{N}}$. This is, however, oftentimes impractical (it is usually impossible to find the explicit formula for the semiclassical expression), so we resort to approximating $\overline{\mathcal{N}}$ as a polynomial of degree d. We find this polynomial by fitting $E_i(i)$. The disadvantages of approximating $\overline{\mathcal{N}}$ as a polynomial will be described in section 2.3.1 on a concrete example.

2.2 Unfolded spectrum as a time series

The unfolded spectrum $\{e_i\}_{i=1}^{N}$ bears some similarities to a *time series*, we can even liken it to a diffusion process of a particle and its random walk. This has been done in [3] and forms the basis of the $1/f$ analysis.

In this analysis, we use the δ_n series defined as

$$\delta_n = e_{n+1} - e_1 - n\,. \tag{2.7}$$

This statistic corresponds to the deviations of eigenenergies from the "smooth" energy (i. e. energy we can attribute to the smooth density). If we set $e_1 = 1$, then we can even write $\delta_n = -\tilde{\mathcal{N}}(E_{n+1})$ [20].

We then interpret δ_n as a time series (and the index n therefore corresponds to time). Next, we calculate the $\hat{\delta}_k$ statistic using the discrete Fourier transform defined as follows (the index k corresponds to frequency):

$$\hat{\delta}_k = \frac{1}{\sqrt{N}} \sum_n \delta_n \exp\left(\frac{-2\pi i k n}{N}\right)\,. \tag{2.8}$$

From $\hat{\delta}_k$ we calculate its power spectrum $S(k)$:

$$S(k) = |\hat{\delta}_k|^2\,. \tag{2.9}$$

Based on [20] we now show some results concerning $S(k)$. Firstly, let us recapitulate the Bohigas-Giannoni-Schmit conjecture. We consider two random matrix ensembles: Gaussian orthogonal ensemble (GOE) and Gaussian unitary ensemble (GUE)[1]. Then, according to the conjecture, the spectrum of a system

[1] There is a third Gaussian ensemble, the Gaussian symplectic ensemble (GSE). It is however not mentioned in [20].

with a chaotic semiclassical analogue exhibits the same statistical properties as a matrix from either the GOE or GUE ensemble (depending on the symmetry of the system). On the other hand, the spectra of systems with integrable classical analogues can be described by Poissonian statistics [21].

From those assumptions, we can derive an equation for $S(k)$ valid for GUE-like spectra and Poissonian statistics and approximately valid for GOE-like spectra:

$$S(k) = \begin{cases} \frac{N^2}{4\pi^2}\left[\frac{K\left(\frac{k}{N}\right)-1}{k^2} + \frac{K\left(1-\frac{k}{N}\right)}{(N-k)^2}\right] + \frac{1}{4\sin^2\left(\frac{\pi k}{N}\right)} - \frac{1}{12} \text{ for chaotic systems,} \\ \frac{N^2}{4\pi^2}\left[\frac{K\left(\frac{k}{N}\right)-1}{k^2} + \frac{K\left(1-\frac{k}{N}\right)}{(N-k)^2}\right] + \frac{1}{4\sin^2\left(\frac{\pi k}{N}\right)} \text{ for integrable systems,} \end{cases} \tag{2.10}$$

where $K(\tau)$ is the spectral form factor defined as

$$K(\tau) = \left\langle \left| \int \tilde{\rho}(e') \exp(-2\pi e\tau) \mathrm{d}e' \right| \right\rangle . \tag{2.11}$$

Using periodic orbit theory and semiclassical mechanics, an expression for $K(\tau)$ can be derived for short times $\tau_{\min} \ll \tau \ll \tau_{\mathrm{H}}$, where $\tau_{\min}$ is the period of the shortest periodic orbit and τ_{H} is the Heisenberg time related to the time a wave packet takes to explore the complete phase space of the system. Then, it holds that

$$K(\tau) = \begin{cases} 1 \text{ for integrable systems,} \\ 2\tau \text{ for GOE-like systems,} \\ \tau \text{ for GUE-like systems.} \end{cases} \tag{2.12}$$

Using eq. (2.12) and assuming $k \ll N$, $N \gg 1$, we can write the Taylor expansion of eq. (2.10):

$$S(k) = \begin{cases} \frac{N^2}{4\pi^2 k^2} \text{ for integrable systems,} \\ \frac{N^2}{2\pi^2 k} \text{ for GOE-like systems,} \\ \frac{N^2}{4\pi^2 k} \text{ for GUE-like systems.} \end{cases} \tag{2.13}$$

We can thus see that $S(k) \propto 1/k^2$ for integrable systems and $S(k) \propto 1/k$ for chaotic systems, which is in accordance with the aforementioned occurence of $1/f$ noise in complex chaotic systems. For systems in between chaoticity and regularity we expect $S(k) \propto 1/k^\alpha$, where $\alpha \in (1, 2)$. We can roughly say that the closer α is to 1, the more chaotic the system is. The coefficient α can thus be used as a chaotic indicator, there is however no straightforward relationship between α and other chaotic indicators such as the *Brody parameter* [22].

Let us add that eq. (2.13) is valid for small k. Near $k = N/2$, the so-called Nyquist frequency, the effects of other terms in (2.10) become apparent and we observe a systematic deviation from linearity—the values of $\log(S(k))$ rise above the predicted linear relationship.

To reiterate, the process of $1/f$ noise analysis goes as follows: we take a Hamiltonian of a system, diagonalise it, unfold the spectrum and construct δ_n. Next we compute $\hat{\delta}_k$ and $S(k)$. Lastly, we fit $\log(S(k))$ as function of $\log(k)$ with a linear function $\log(S(k)) = \alpha \log(k) + \beta$. The coefficient α is the result, it tells us something about the chaoticity of the observed system.

2.3 Caveats of $1/f$ noise analysis

It is relatively simple to implement $1/f$ noise analysis, but less so to verify its correctness and to interpret the results. Let us now consider an example system consisting of a random diagonal matrix (with uniform distribution) of dimension $d = 30\,000$ with elements $\lambda_i \in [0, d]$ and analyse its spectrum.

We do not unfold the spectrum because the smooth level density is already $\overline{\rho}(e) = 1$. After conducting $1/f$ noise analysis in section 2.2, we obtain a power spectrum depicted in fig. 2.1. The resulting dependency portrayed in the graph is indeed linear with the exception of the "tail" for high k. This increase of power spectrum for high k in accordance with predictions stemming from random matrix theory described in section 2.2, in particular with eq. (2.10), and is also described in [20].

When fitting, we therefore have to ignore data for k greater than certain $k_{\max}$. There is no formula for determining $k_{\max}$, one therefore has to err on the side of caution. Usually about 1/3 to 1/2 of the frequencies are considered for the fit. With a correct fit, we see that $\alpha = 2$ for the system is integrable.

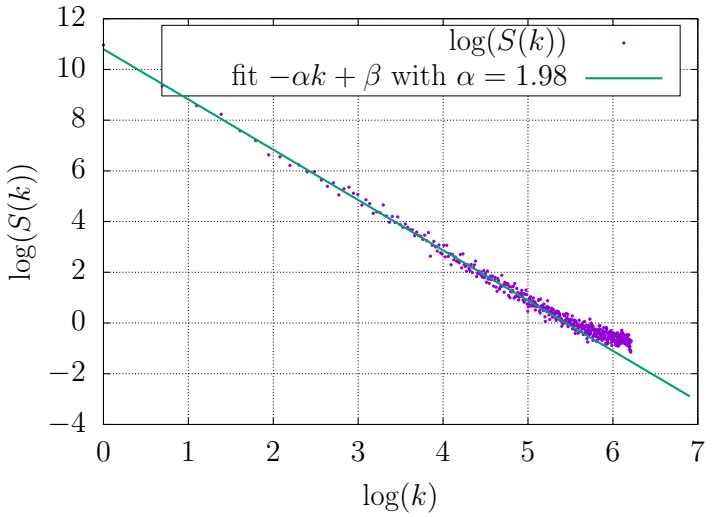

Figure 2.1: Power spectrum of a diagonal matrix with $d = 30\,000$.

2.3.1 Unfolded spectrum

We now unfold the eigenenergies of a new diagonal matrix constructed as described in section 2.1. $1/f$ noise analysis yields a power spectrum depicted in fig. 2.2. We notice that the dependency is again not completely linear. Deviation from linearity for high k has been discussed in section 2.3, but now there is a new deviation for low k.

This deviation has been caused by imperfect polynomial unfolding [18, fig. 3]—it is possible to "overfit" the $\overline{\mathcal{N}}(E)$ and include in it even long range correlations. This removes small frequencies from the $\hat{\delta}_k$ time series, which manifests itself in a lower value of $S(k)$ for small k. The higher the degree of the polynomial used for fitting, the more severe this problem becomes. We therefore have to ignore unphysical values of $S(k)$ in our fit and start fitting from $k_{\min}$ (just as we fit up to a certain $k_{\max}$). Preferably, we also don't use polynomials of a very high degree.

Another reason for having to set $k_{\min}$ and $k_{\max}$ was outlined in sec. 2.2. The fundamental equation (2.13) is valid only for certain $\tau_{\min}$ and $\tau_{\max}$, which influence $k_{\min}$ and $k_{\max}$. This limitation doesn't manifest itself in fig. 2.2 as the system was already generated with the desired spectral characteristics. It shall, however, cause problems in real analysis, for in practice determining times $\tau_{\min}$ and $\tau_{\max}$ is impossible or impractical. We will have to suitably choose $k_{\min}$ and $k_{\max}$.

Lastly, no polynomial is bounded at $\pm\infty$, so the fit doesn't represent the actual $\overline{\mathcal{N}}(E)$ well at the edges of the spectrum [18]. We therefore remove some eigenlevels from the high and low end of the spectrum to improve the fit. We call this *cutting*.

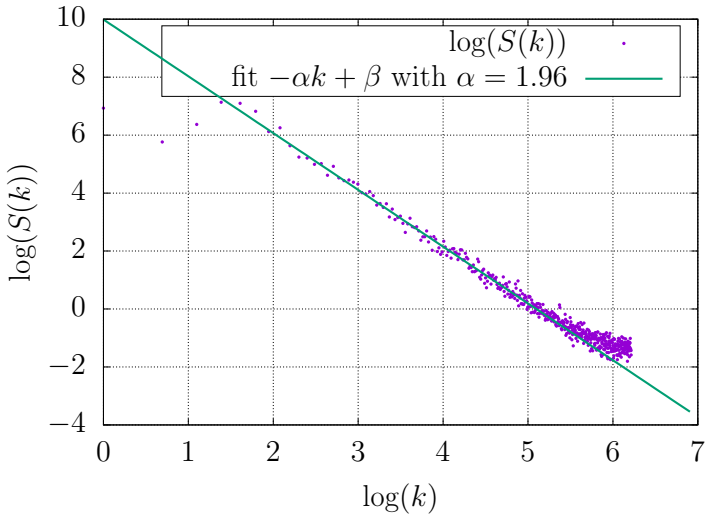

Figure 2.2: Power spectrum of a diagonal matrix with $d = 30\,000$, energies were unfolded.

3. The Vibron Model

In the previous chapter we went over the description of general quantum systems. The focus of this chapter will be the introduction of one particular system called *the Vibron model*. This system was first introduced in [9], where it was shown that it can be used to describe linear or bent molecules. The vibron model is a finite integrable system, so in the end we will show how to modify it with a chaotic perturbation and proceed to use this modified system for our study of quantum chaos.

Thanks to its relative simplicity, it is feasible to understand how the vibron model works, which makes it easier to determine the efficacy of the $1/f$ noise description of chaos. Furthemore, a classical limit of this system has been already described in [10, 23], which will also prove useful.

In particular, the vibron model depicts the *bending vibrations* of linear polyatomic molecules. In such a molecule oriented along the z-axis it describes the vibrations of one atom in the xy plane. The model has also been used to describe a Bose-Einstein condensate of ^{87}Rb atoms in [24]. To keep matters clear, we shall hold on to the polyatomic molecule interpretation though.

3.1 Group theoretical background

Despite its utility in chemistry, the vibron model is not empirical. Rather, it is a so-called *algebraic model*, which means that it is tied to the group theory. The process of constructing an algebraic model goes rougly as follows. Firstly, we choose a particular symmetry group (a *Lie group*), in our case $U(3)$. Next, we take its *Lie algebra*, in our case the $u(3)$ algebra. Then we consider the elements of $u(3)$ (as abstract mathematical concepts) and try to find a correspondence between them and quantum-mechanical operators (as concrete observables with a physical interpretation). If all goes well, the resulting Hamiltonian is constructed using the operators connected to the Lie algebra and should be invariant under the desired physical symmetry. A more comprehensive explanation of algebraic models is presented in [25].

In the case of the vibron model, an important concept is the Hilbert space of k bosonic excitations $\mathcal{H}^{(k)}$. The direct sum of $\mathcal{H}^{(k)}$ for all k is called the Fock space [12]. In this space we can introduce bosonic creation and annihilation operators $\hat{b}_k$ and $\hat{b}_k^+$ with the following commutation relations:

$$\left[\hat{b}_i, \hat{b}_j^+\right] = \delta_{ij}\,, \ \left[\hat{b}_i, \hat{b}_j\right] = 0\,. \tag{3.1}$$

Two boson operators $\hat{\tau}_x$, $\hat{\tau}_y$ together with a scalar boson operator $\hat{\sigma}$ can be used to define nine operators $\hat{b}_i^+\hat{b}_j$ that form the $u(3)$ algebra. In [9] and [26] hermitean linear combinations of $\hat{b}_i^+\hat{b}_j$ are used for convenience. The operators we need for our analysis are listed in table 3.1.

Let us note that in principle the Hamiltonian we get from an algebraic model is a Hamiltonian in the second quantized form. In our case, we will only have a Hamiltonian with up to 2-body interactions, which can be described by the

following equation [12]:

$$\hat{H}_{2q} = \sum_{i,i'} \epsilon_{ii'} \hat{b}_i^+ \hat{b}_{i'} + \frac{1}{2} \sum_{\substack{ij \\ i'j'}} \nu_{iji'j'} \hat{b}_i^+ \hat{b}_j^+ \hat{b}_{j'} \hat{b}_{i'} \,. \tag{3.2}$$

Operator	Bosonic expression	Name
$\hat{n}$	$\hat{\tau}_+^+\hat{\tau}_+ + \hat{\tau}_-^+\hat{\tau}_-$	number of vibrational quanta
$\hat{l}$	$\hat{\tau}_+^+\hat{\tau}_+ - \hat{\tau}_-^+\hat{\tau}_-$	rotation along the z-axis
$\hat{D}_+$	$\sqrt{2}(\hat{\tau}_+^+\hat{\sigma} - \hat{\sigma}^+\hat{\tau}_-)$	+ dipole operator
$\hat{D}_-$	$\sqrt{2}(-\hat{\tau}_+^+\hat{\sigma} + \hat{\sigma}^+\hat{\tau}_-)$	− dipole operator
$\hat{D}_x$	$\frac{1}{2}\left(\hat{D}_+ + \hat{D}_-\right)$	x dipole operator
$\hat{R}_+$	$\sqrt{2}(\hat{\tau}_+^+\hat{\sigma} + \hat{\sigma}^+\hat{\tau}_-)$	transformed + dipole operator
$\hat{R}_-$	$\sqrt{2}(\hat{\tau}_+^+\hat{\sigma} + \hat{\sigma}^+\hat{\tau}_-)$	transformed − dipole operator
$\hat{R}_x$	$\frac{1}{2}\left(\hat{R}_+ + \hat{R}_-\right)$	transformed x dipole operator

Table 3.1: Table of used operators and their definitions in terms of $\hat{\tau}_+$, $\hat{\tau}_-$ and $\hat{\sigma}$ [9].

3.2 The Hamiltonian

There are two so-called *subalgebra chains* of interest:

1. $u(3) \supset u(2) \supset o(2)$: the cylindrical oscillator chain I,
2. $u(3) \supset o(3) \supset o(2)$: the displaced oscillator chain II.

A Hamiltonian formed from the *Casimir operator* of a Lie algebra is invariant under the symmetry of the corresponding Lie group. A Hamiltonian comprising of linear and quadratic Casimir operators of the algebras in both presented subalgebra chains will thus have the symmetry of the last link in the subalgebra chain—the $O(2)$ group symmetry. This means it will be invariant under rotation, which is the symmetry of our problem. Such a Hamiltonian looks as follows [9]:

$$\begin{aligned} \hat{H}_{\text{gen}} &= E_0 + \epsilon\hat{C}_1[u(2)] + \alpha\hat{C}_2[u(2)] + \beta\hat{C}_2[o(2)] + A\hat{C}_2[o(3)] \\ &= E_0 + \epsilon\hat{n} + \alpha\hat{n}(\hat{n}+1) + \beta\hat{l}^2 + A\hat{W}^2 \,. \end{aligned} \tag{3.3}$$

In the first line, the Hamiltonian is written in terms of linear (C_1) and quadratic (C_2) Casimir operators of the algebras in brackets. The Casimir operators are expressed explicitly in the second line: E_0, ϵ, α and β are constants, $\hat{n}$ is the operator of the number of vibrational quanta and $\hat{l}$ is the operator of rotation along the z-axis. The operator $\hat{W}^2$ can be expressed using dipole operators $\hat{D}_\pm$ as follows:

$$\hat{W}^2 = \frac{1}{2}\left(\hat{D}_+\hat{D}_- + \hat{D}_-\hat{D}_+\right) + \hat{l}^2 \,. \tag{3.4}$$

If we adjust $\hat{H}_{\text{gen}}$ for cylindrical symmetry, we obtain the following Hamiltonian:

$$\hat{H}_{\text{I}} = E_0 + \epsilon\hat{n} + \alpha\hat{n}(\hat{n}+1) + \beta\hat{l}^2 \,. \tag{3.5}$$

This Hamiltonian corresponds to chain I and it represents a fully linear molecule. If we, on the other hand, put restrictions on $\hat{H}_{\text{gen}}$ in line with chain II, we obtain the following Hamiltonian:

$$\hat{H}_{\text{II}} = E_0 + A\hat{W}^2 + \beta\hat{l}^2 \,. \tag{3.6}$$

This Hamiltonian corresponds to a linear molecule, where the observed atom is displaced from its place in the molecule.

The Hamiltonian of the vibron model represents a quantum phase transition between $\hat{H}_{\text{I}}$ and $\hat{H}_{\text{II}}$, it is still invariant under the $O(2)$ symmetry. It takes the following form:

$$\hat{H}_{\text{tr}} = (1-\xi)\hat{n} - \frac{\xi}{(N-1)}\hat{W}^2 \,, \tag{3.7}$$

where $\xi \in [0,1]$ represents the quantum phase transition parameter and N is the number of bound states (vibrons).

As the vibron model is integrable, we must break its integrability to observe chaos. We do this by introducing another dipole operator $\hat{D}_x = (\hat{D}_+ + \hat{D}_-)/2$, which results in the following Hamiltonian:

$$\hat{H}_D = (1-\xi)\hat{n} - \frac{\xi}{(N-1)}\hat{W}^2 + c\hat{D}_x \,, \tag{3.8}$$

where $c \in \mathbb{R}^+$ is the perturbation parameter.

3.2.1 Calculating the spectrum

We use the basis of a cylindrical oscillator for our calculations. This basis arises from the subalgebra chain I. Its basis elements are the eigenvectors of $\hat{H}_{\text{I}}$, which can be written as $|N\,n\,l\rangle$. The quantum numbers can take the following values:

- $N \in \mathbb{N}^+$,
- $n = 0,\, 1,\, \ldots,\, N$ and
- $l = \pm n,\, \pm(n-2),\, \ldots,\, 0$.

Matrix elements of individual operators expressed in the cylindrical oscillator basis are [9, 26]:

$$\langle N'\,n'\,l'|\hat{n}|N\,n\,l\rangle = \delta_{N',N}\delta_{n',n}\delta_{l',l}\,n \,, \tag{3.9}$$

$$\begin{aligned}\langle N'\,n'\,l'|\hat{W}^2|N\,n\,l\rangle &= \delta_{l,l'}\delta_{N,N'}\delta_{n',n+2}\sqrt{(N-n)(N-n-1)(n+l+2)(n-l+2)} \\ &\quad + \delta_{l,l'}\delta_{N,N'}\delta_{n',n}\left[(n^2-l^2)+(N-n)(N-n-1)\right] \,,\end{aligned} \tag{3.10}$$

$$\begin{aligned}\langle N'\,n'\,l'|\hat{D}_x|N\,n\,l\rangle &= \delta_{N',N}\delta_{n',n+1}\delta_{l',l+1}\frac{\sqrt{2}}{2}\sqrt{(n+l+2)(N-n)} \\ &\quad - \delta_{N',N}\delta_{n',n+1}\delta_{l',l-1}\frac{\sqrt{2}}{2}\sqrt{(n-l+2)(N-n)} \,.\end{aligned} \tag{3.11}$$

Since

$$\langle N'n'l'|\hat{H}_D|Nnl\rangle \propto \delta_{NN'}\,, \tag{3.12}$$

we will study the eigenenergies for just one N. This corresponds to taking the Hamiltonian $\hat{H}_D|_N$, which is $\hat{H}_D$ reduced to the subspace of a particular value of N.

To showcase the transition between the two limiting cases $\xi = 0$ and $\xi = 1$ of $\hat{H}_D$, we have made the so-called *correlation diagrams* for systems with and without perturbation. Those diagrams describe how energies of eigenstates change when we transition from cylindrical oscillator chain I to chain II[1] [9]. The diagrams are displayed in fig. 3.1.

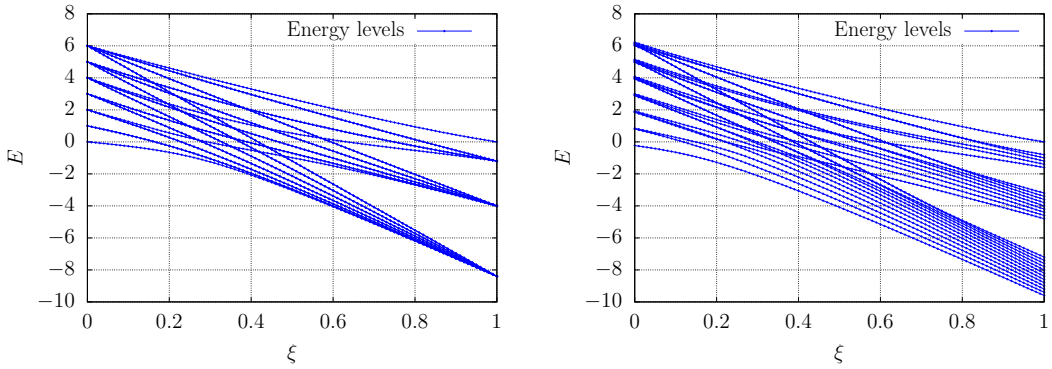

(a) Without perturbation ($c = 0.0$) (b) With perturbation ($c = 0.2$)

Figure 3.1: Correlation diagrams of the vibron model for $N = 6$ with and without perturbation; individual energies are joined with lines for visual clarity.

Let us remark that for $c = 0$ degeneracies at $\xi = 0$ or $\xi = 1$ are introduced. This is due to either the first or second term in eq. (3.8) vanishing, which results in a higher symmetry of the problem—the transition to the chain I (or II) is complete. With $c > 0$, the degeneracy is lifted by the perturbation—$\xi = 0, 1$ do not simpify the Hamiltonian enough.

3.3 The Z_2 symmetry

Instead of the dipole operators $\hat{D}_\pm$, the operators $\hat{R}_\pm$ can be used in the Hamiltonian $\hat{H}_D$. This corresponds to the transformation

$$\hat{\tau}_- \leftrightarrow -\hat{\tau}_-\,, \tag{3.13}$$

$$\text{which manifests itself as } \hat{W}^2 \to \hat{W}_R^2 = \frac{1}{2}\left(\hat{R}_+\hat{R}_- + \hat{R}_-\hat{R}_+\right) + \hat{l}^2\,. \tag{3.14}$$

The operators $\hat{R}_\pm$ are listed in table 3.1 with other operators for comparison.

The transformation from eq. (3.14) has no impact on the spectrum as can be seen from the second quantisation form of the Hamiltonian $\hat{H}_D$, which is

[1] In terms of the polyatomic linear molecule interpretation, this corresponds to the equilibrium position of the described atom changing from being along the z-axis of the molecule to being off the axis.

expressed in eq. (3.2). Let us illustrate this for a case of a single body interaction Hamiltonian:

$$\hat{H}_1 = \sum_{i,i'} \epsilon_{ii'} \hat{b}_i^+ \hat{b}_{i'} \Rightarrow E_k = \langle E_k | \hat{H}_1 | E_k \rangle = \langle E_k | \sum_{i,i'} \epsilon_{ii'} \hat{b}_i^+ \hat{b}_{i'} | E_k \rangle \,, \tag{3.15}$$

where $\hat{b}_i$ is $\hat{\sigma}$, $\hat{\tau}_+$ or $\hat{\tau}_-$ for $i = 1, 2, 3$, E_k is an eigenenergy and $|E_k\rangle$ is its eigenstate. Let us express the eigenstates in terms of the basis $|abc\rangle$, where a, b, c are bosons corresponding to the individual boson operators. We then get:

$$E_k = \sum_{\substack{abc \\ a'b'c'}} \sum_{i,i'} \alpha_{abc} \overline{\alpha}_{a'b'c'} \epsilon_{ii'} \langle a'b'c' | \hat{b}_i^+ \hat{b}_{i'} | abc \rangle \,. \tag{3.16}$$

If we interchange $\hat{\tau}_-$ for $-\hat{\tau}_-$, we get:

$$\hat{H}_2 = \sum_{i,i'} \epsilon_{ii'} \hat{b}_i^+ \hat{b}_{i'} (-1)^{\delta_{i3} + \delta_{i'3}} \,, \tag{3.17}$$

where δ is the Kronecker delta. Now, if we modify eigenvectors $|E_k\rangle$ of $\hat{H}_1$, we will get eigenvectors $|E_k^-\rangle$ for $\hat{H}_2$ with the same eigenenergies. We proceed as follows:

$$|E_k\rangle = \sum_{abc} \alpha_{abc} |abc\rangle \;\rightarrow\; |E_k^-\rangle = \sum_{abc} \alpha_{abc} |abc\rangle (-1)^c \tag{3.18}$$

$$\begin{aligned} E_k = \langle E_k | \hat{H}_1 | E_k \rangle &= \sum_{\substack{abc \\ a'b'c'}} \sum_{i,i'} \alpha_{abc} \overline{\alpha}_{a'b'c'} \epsilon_{ii'} \langle a'b'c' | \hat{b}_i^+ \hat{b}_{i'} | abc \rangle \\ &\rightarrow \\ E_k \stackrel{?}{=} \langle E_k^- | \hat{H}_2 | E_k^- \rangle &= \sum_{\substack{abc \\ a'b'c'}} \sum_{i,i'} \alpha_{abc} \overline{\alpha}_{a'b'c'} \epsilon_{ii'} \langle a'b'c' | \hat{b}_i^+ \hat{b}_{i'} | abc \rangle (-1)^{\delta_{i3} + \delta_{i'3} + c + c'} \,. \end{aligned} \tag{3.19}$$

we now note that:

- if $c = c'$, then the only nonzero $\langle abc | \hat{b}_i^+ \hat{b}_{i'} | a'b'c' \rangle$ is for $\delta_{i3} = \delta_{i'3}$,
- if $c = c' \pm 1$, then the only nonzero $\langle abc | \hat{b}_i^+ \hat{b}_{i'} | a'b'c' \rangle$ is for $\delta_{i3} \neq \delta_{i'3}$,
- if $c = c' \pm k$, where $k \neq 1$, then $\langle abc | \hat{b}_i^+ \hat{b}_{i'} | a'b'c' \rangle = 0$.

From this it follows that $\langle E_k^- | \hat{H}_2 | E_k^- \rangle = E_k$. A similar argument can be made for a general form in the 2nd quantisation form. We have thus shown that the Hamiltonian

$$\hat{H}_R = (1 - \xi)\hat{n} - \frac{\xi}{(N-1)} \hat{W}_R^2 + c\hat{R}_x \tag{3.20}$$

has the same eigenvalues as the Hamiltonian $\hat{H}_D$. Furthemore, this Hamiltonian exhibits a Z_2 (sometimes called mirror or parity) symmetry [24]—it is invariant to the interchange $l \rightarrow -l$. We have plotted the heatmaps of Hamiltonians $\hat{H}_D$ and $\hat{H}_R$ in fig. 3.2 for illustrative purposes.

There exists a basis adapted to the Z_2 symmetry, in which $\hat{H}_R$ is block diagonal. Eigenstates from different blocks are not correlated, wherefore it makes sense to

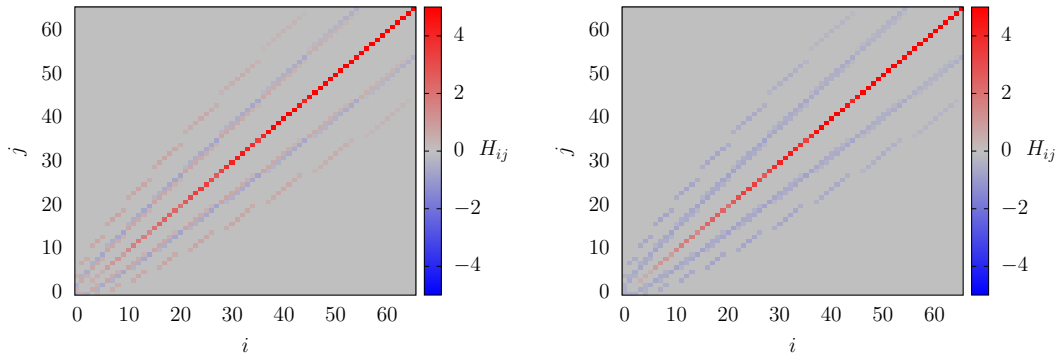

(a) Hamiltonian $\hat{H}_D$ (b) Hamiltonian $\hat{H}_R$

Figure 3.2: Heatmaps of two of the used Hamiltonians expressed as matrices in the $|N, n, l\rangle$ basis. We chose the parameters $N = 10$, $\xi = 0.2$ and $c = 0.2$. A small dimension has been chosen for visual clarity.

analyse the spectra of both blocks separately—if we didn't do it, we would include unphysical correlations into our analysis, which would skew it. We can write the Z_2 symmetry adapted basis as follows (it is trivial to verify that its states are invariant to the interchange $l \to -l$):

$$\left\{ \frac{1}{\sqrt{2}} \left(|N, n, l\rangle + |N, n, -l\rangle \right), \frac{1}{\sqrt{2}} \left(|N, n, l\rangle - |N, n, -l\rangle \right) \right\} \equiv \{ |\psi^+\rangle, |\psi^-\rangle \} . \tag{3.21}$$

Usually about half of the basis states are $|\psi^+\rangle$ and half $|\psi^-\rangle$. The number of $|\psi^+\rangle$ states is a bit higher as states $|N, n, 0\rangle$ count as $|\psi^+\rangle$. The transformation from $\{|N, n, l\rangle\}$ to $\{|\psi^+\rangle, |\psi^-\rangle\}$ can be done through a unitary matrix, it therefore also preserves eigenvalues.

To determine, whether an eigenvalue belongs to a vector $|\psi^+\rangle$ or $|\psi^-\rangle$, we do not have to transform the basis though. Let us consider a certain energy state E_j and a corresponding eigenstate $|\psi_j\rangle$. We can expand $|\psi_j\rangle$ into the basis $|N, n, l\rangle$ thusly:

$$|\psi_j\rangle = \sum_{n,l} c_{nl}^{(j)} |N, n, l\rangle . \tag{3.22}$$

We can now calculate the projection $\langle \psi_j | \psi^\pm \rangle$. If $\langle \psi_j | \psi^+ \rangle = 0$, then $|\psi_j\rangle \in \{|\psi^-\rangle\}$ and vice versa. We can then formulate a simple condition:

$$\langle \psi_j | \psi^+ \rangle = \sum_{n,l>0} \left[c_{nl}^{(j)} + c_{n-l}^{(j)} \right] = 0 \text{ for } |\psi_j\rangle \in \{|\psi^-\rangle\} , \tag{3.23}$$

$$\langle \psi_j | \psi^- \rangle = \sum_{n,l>0} \left[c_{nl}^{(j)} - c_{n-l}^{(j)} \right] = 0 \text{ for } |\psi_j\rangle \in \{|\psi^+\rangle\} . \tag{3.24}$$

Of course, the equations will hold only approximately when tested numerically. In the case of $c = 0$, the x dipole term $\hat{R}_x$ disappears from the Hamiltonian, degeneracies are introduced and the above procedure is no longer valid. We can only remove duplicit eigenvalues from the spectrum and obtain just one graph.

3.3.1 Impacts of the symmetry on $1/f$ noise analysis

$1/f$ analysis is more accurate, if we conduct it separately for $\{|\psi^+\rangle\}$ and $\{|\psi^-\rangle\}$. We then get two graphs with a very concrete interpretation: they represent the chaoticity of two independent subspaces of the phase space of our problem. The phase subspaces can even be visualised in the classical limit with the help of Poincaré sections (see [10, fig. 2.9]). One important difference between the classical limit and the quantum case is that $\{|\psi^+\rangle\}$ contains states with $l = 0$ and thus has more states than $\{|\psi^-\rangle\}$. This difference diminishes as we approach the classical limit for $N \to \infty$.

4. Numerical results

In the previous chapter we introduced the perturbed vibron model. We will be analysing its Hamiltonian $\hat{H}_D$ in the $|N, n, l\rangle$ basis from eq. (3.8) in terms of the $1/f$ noise method described in the first chapter. To calculate the spectrum of the Hamiltonian we used the cylindrical oscillator basis $|N, n, l\rangle$. Subsequently, we will be analysing two blocks of the transformed Hamiltonian $\hat{H}_R$ from eq. (3.20) for more relevant results.

The vibron model has a finite Hilbert space of dimension $\dim = N(N+1)/2$. This is in some sense an advantage as we are able to express the Hamiltonian exactly—in the case of infinite Hilbert spaces we would only be able to approximate it. It is still more accurate to analyse a Hamiltonian with a large dimension, because a large dimension means denser spectrum[1] and that in turn makes it easier to examine spectral statistics.

4.1 Chaoticity for different c

For this analysis we chose $N = 120$ ($\dim = 7\,381$) as the Hamitonian has a sufficiently large dimension but is still relatively easily diagonalisable. Furthemore, we took $\xi = 0.2$, as the classical limit of a Hamiltonian with similar parameters has been examined in [10], p. 45. Moreover, the parameter $\xi = 0.2$ is at the quantum phase transition[2]. Next we chose multiple values of c and analysed the resulting Hamiltonian—the point was to find out which values of c are the most chaotic.

The system is integrable for $c = 0$, so we expect that $1/f$ noise analysis will confirm this ($\alpha \approx 2$). With c increasing, the perturbation makes the system more chaotic and this should be reflected in our analysis too ($\alpha \to 1$). We should only observe chaoticity only to a certain point however. For as $c \gg 1$, the dipole operator stops being a perturbation and it starts "dominating" the Hamiltonian: the system returns to integrability. We have chosen the range $c \in [0, 1]$, as a compromise between a dense sampling and a large range.

The basic procedure of our analysis is as follows:

Step 1: Using equations (3.9), (3.10) and (3.11) we construct the Hamiltonian from eq. (3.8) and compute its eigenvalues with a routine `dsyev` from LAPACKe.

Step 2: We cut the lowest and the highest 200 eigenlevels.

Step 3: We choose an integer `window`, in our case[3] `window`=512.

Step 4: We split eigenenergies into intervals of length `window`. For each interval we:

(a) unfold the energies as described in section 2.1 (polynomial of degree 8 was used),

(b) *stretch* the energies, i. e. subtract from them a number and multiply them so that the lowest energy becomes 0 and the highest `window`,

[1] The limit $N \to \infty$ is the classical limit with a continuous spectrum.

[2] For more information on quantum phase transition see [27].

[3] In some other works on $1/f$ noise, `window`=256 was chosen [**?** 4].

(c) calculate the power spectrum $S(k)$ as described in section 2.2 and save it in an array `powerspec`.

Step 5: Calculate the average of all arrays `powerspec[]` and store them in a new array `powerspecavg[]`.

Step 6: Plot the logarithm of the averaged power spectrum from `powerspecavg[]` as a function of the logarithm of the array index. Fit[4] this graph with a linear function $y = -\alpha x + \beta$. The coefficient α is the desired chaos indicator.

The results of this analysis can be seen in figure 4.1. We see that even for $c = 0$ our analysis doesn't indicate integrability as $\alpha < 2$. For larger c, the chaoticity increases, but doesn't behave as in [10] (figures 2.24 and 2.25). This may be due to the fact that we work with a slightly different Hamiltonian—in [10] two parameters in place of our ξ are used. Moreover, there is no straightforward relationship between α as a chaos indicator and other chaos indicators let alone classical chaos indicators (see sec. 2.2). Additionally, our values of c weren't high enough for the vibron model to return to integrability.

Let us now comment on the accuracy of the method. We see that we had to omit lower frequencies from the fit as was outlined in sec. 2.3. We tried varying the order of the polynomial used for unfolding, but it didn't have much influence on the appearance of unphysical frequencies indicating that they do not stem from the approximation of $\overline{\mathcal{N}}$. Frequencies on the higher end of the spectrum were also ignored as they are explainable by the theoretical derivation of $1/f$ noise (see section 2.2).

Nevertheless, after ignoring frequencies at the higher and lower end, we are left with data that visually correspond to the predicted linear relationship. This relationship is clearer in less chaotic systems (as in fig. 4.1 (a)) and less pronounced in more chaotic systems (as in fig. 4.1 (c)). We believe that the accuracy of our fits could be improved by choosing higher N, which would mean more data used for the fit. We have tried to estimate errors of α, which will be discussed in the following section 4.2.

4.2 Inclusion of the Z_2 symmetry

As we have written in section 3.3, the analysed Hamiltonian has a Z_2 symmetry which we should incorporate into our analysis. If we don't do it, as we haven't done in section 4.1, it may disturb the real, physical correlations (see section 3.3.1). From this section on we shall therefore conduct the same analysis as in section 4.1, but for the two subspaces $\{|\psi^+\rangle\}$ and $\{|\psi^-\rangle\}$ (the splitting of eigenvalues into two subspaces has been done as in section 3.3). The rest of the procedure is similar to the process outlined in section 4.1 with the notable exception of taking `window` $= 256$ (we were able to do this because we had fewer eigenvalues to analyse). The results for $c > 0$ are in figures 4.2 and 4.3.

We expect the results for $|\psi^+\rangle$ and $|\psi^-\rangle$ as they correspond to the same classical system and thus should exhibit the same spectral characteristics according to

[4]For fitting we have used a nonlinear least squares Levenberg–Marquardt algorithm implemented in Gnuplot.

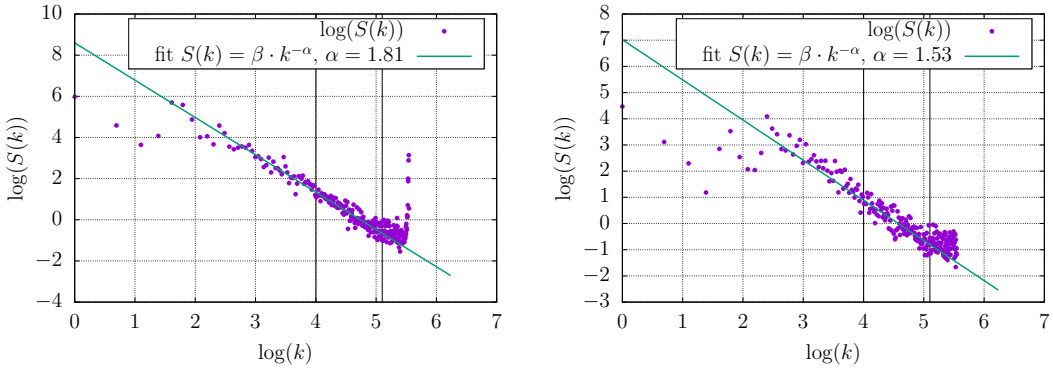

(a) $c = 0.0$

(b) $c = 0.2$

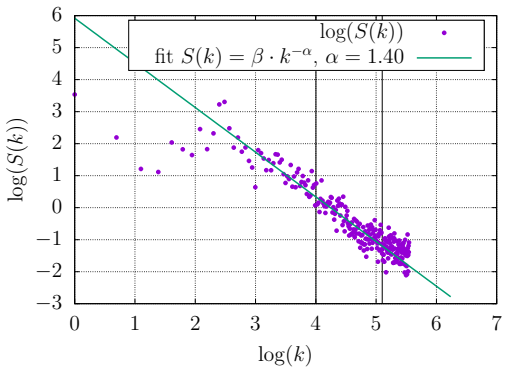

(c) $c = 0.4$

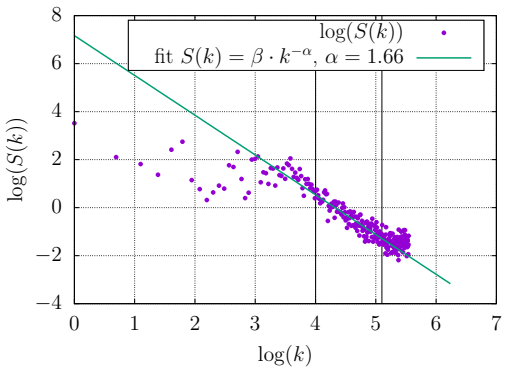

(d) $c = 0.6$

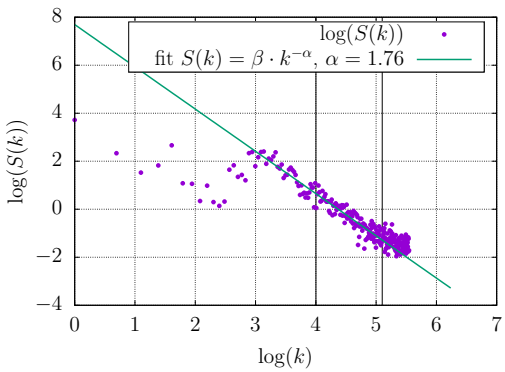

(e) $c = 0.8$

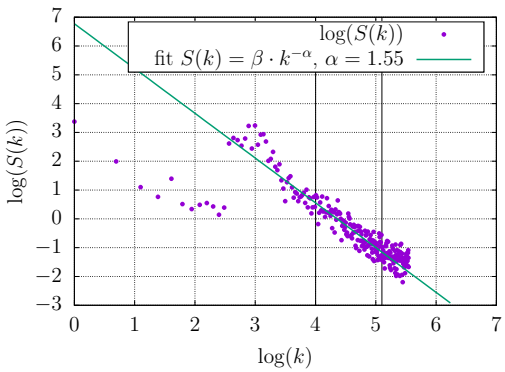

(f) $c = 1.0$

Figure 4.1: Power spectra of vibron models for $N = 120$, dim $= 7\,381$, $\xi = 0.2$ and c from 0.0 to 1.0. Vertical lines indicate fitting range.

the Bohigas conjecture. All in all, the two values should help us obtain a more meaningful estimate of α and the difference between α^+ and α^- could serve as an error estimate.

For $c = 0$ we get similar results to section 4.1. In other cases, $\alpha^\pm$ differ from α, but follow the same general pattern. To get an overview of the data, we made a graph of different α coefficients as a function of c (fig. 4.4). There were two sources of error: firstly the fitting errors from our program. Secondly, another source of error comes from the inability to accurately determine the fitting range—even a small variation in it changes α. We have estimated the two errors to be approximately equal, so as the resulting error we took the fitting error times $\sqrt{2}$.

We see that α^+ and α^- are always close within error bars, but are further

from α. Still, the relationship between α^+, α^- and α is not very conclusive due to very high errors.

When we compare graphs from this section to graphs from section 4.1, we see that visually, the linear relationships in section 4.1 are more convincing, as the deviation of individual points from the fit is not as high. This may be caused by the fact that there are less states to analyse, because we had split the total number of states into two subspaces. We had to take a two times smaller `window` (due to having used approximately half of the states), but this resulted in us not being able to register correlations of longer range. We expect the linear relationships to be more pronounced for greater N and greater `window`, which we couldn't afford to use due to computational restrictions.

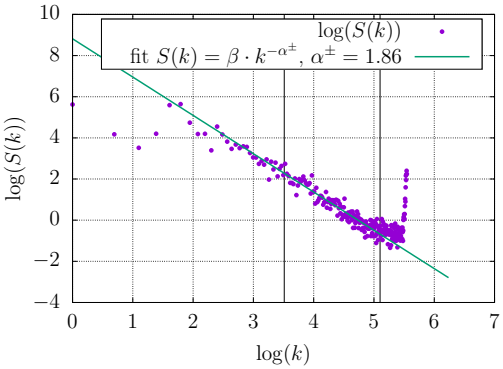

(a) $c = 0.0$

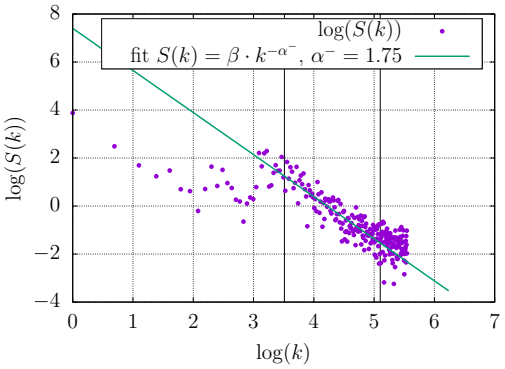

(b) $|\psi^+\rangle$, $c = 0.2$

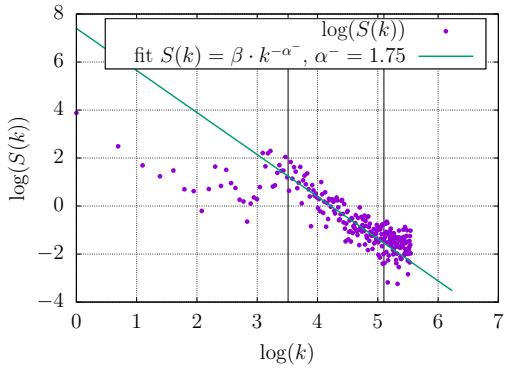

(c) $|\psi^-\rangle$, $c = 0.2$

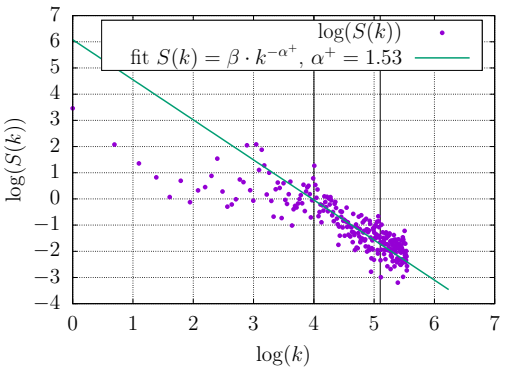

(d) $|\psi^+\rangle$, $c = 0.4$

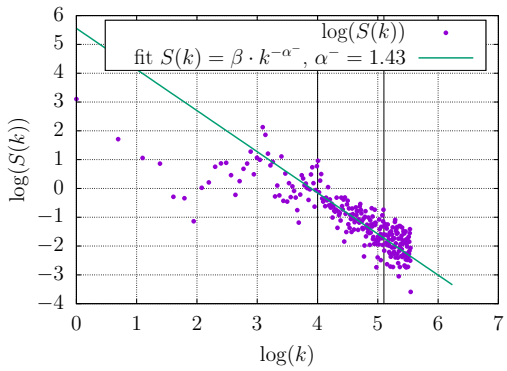

(e) $|\psi^-\rangle$, $c = 0.4$

Figure 4.2: Power spectra of the vibron model for $N = 120$, dim $= 7\,381$, $\xi = 0.2$ and c from 0.0 to 0.4. Vertical lines indicate fitting range.

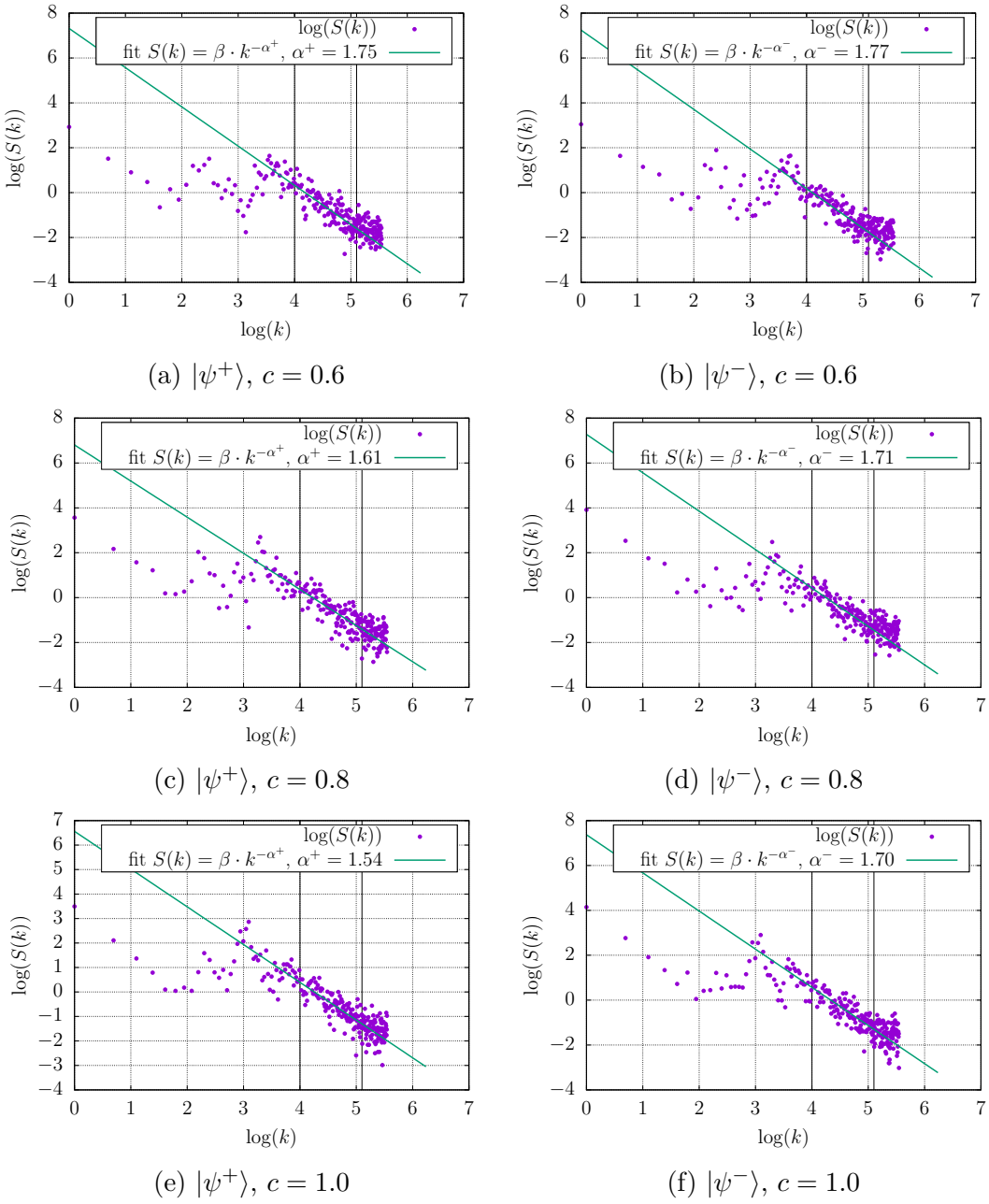

(a) $|\psi^+\rangle$, $c = 0.6$ (b) $|\psi^-\rangle$, $c = 0.6$

(c) $|\psi^+\rangle$, $c = 0.8$ (d) $|\psi^-\rangle$, $c = 0.8$

(e) $|\psi^+\rangle$, $c = 1.0$ (f) $|\psi^-\rangle$, $c = 1.0$

Figure 4.3: Power spectra of the vibron model for $N = 120$, dim $= 7\,381$, $\xi = 0.2$ and c from 0.6 to 1.0. Vertical lines indicate fitting range.

We still don't observe integrability ($\alpha \approx 2$) for $c = 0$ in fig. 4.2 (a), which goes against the predictions of the theory. Furthemore, we have observed that at the end of the spectrum, the intensity of frequencies increased drastically. We do not think this is due to the predicted increase which was described in section 2.3, but rather due to a presence of other correlations. We have ignored the deviating frequencies from our fit, but we presume that other frequencies could have been affected by this correlation too. This is however hypothetical, the effect needs further investigation.

Another problem that we encountered during our analysis were states, for which neither 3.23 nor 3.24 held. This was always the case for two states with consecutive values l, which had the same energy. In case of such a degeneracy, the

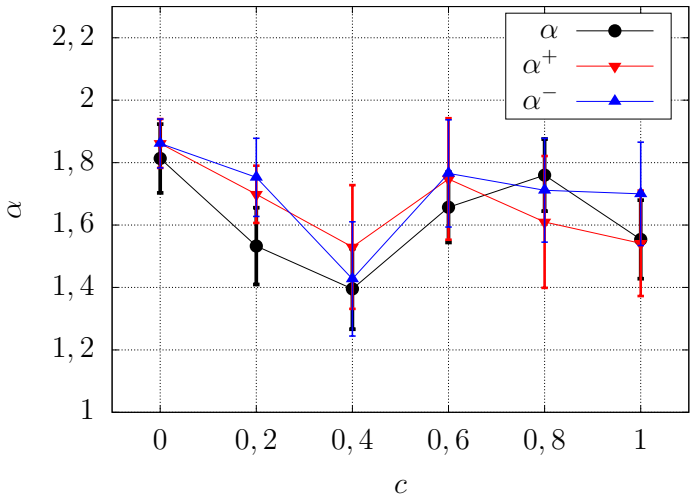

Figure 4.4: The dependence of α on c for $\xi = 0.2$. Points were joined with lines for greater legibility.

diagonalistion procedure didn't produce eigenvectors that were strictly either in $\{|\psi^+\rangle\}$ or in $\{|\psi^-\rangle\}$. We resolved this by putting the degenerate energy in both $\{|\psi^+\rangle\}$ and $\{|\psi^-\rangle\}$.

4.3 Chaoticity for different ξ

Next we analysed the vibron model for a constant $c = 0.4$—the most chaotic value that we have registered in our longitudal analysis, which can be seen from fig. 4.4. This analysis consisted in varying ξ to figure out, which set of parameters is the most chaotic. The resulting graphs for individual ξ and c are in figures 4.6 and 4.5. An overview of different coefficients α is in fig. 4.7.

As we see from the comparison of fig. 3.1 (a) and (b), the degeneracies for $\xi = 0$ and $\xi = 1$ are not much perturbed by a small c. For instance for $\xi = 0$, the system exhibits a close to equidistant spectrum (as in a harmonic oscillator). This should make the signs of chaoticity less apparent and our analysis less conclusive. Thus, as can be seen from fig. 4.6, the graphs (a), (b), (c) and (d) don't seem to exhibit any linearity. We therefore consider the analysis invalid and do not produce a fit. Nevertheless, we believe that the results could be improved if we chose a larger N, because that would provide us with more data and the expected relationship would become clearer. Another way of improving the analysis is taking systems with similar N. This will be discussed in later sections.

For other values of ξ, the analysis doesn't suffer from the same problems and indeed is more conclusive as can be seen from fig. 4.5. Yet, errors in α are very high as is the case for $\xi = 0.4$, for which the value of α in error range is almost the whole interval from 1 to 2. We see that $\alpha^\pm$ are approximately the same (within error range) for all values of ξ. This is to be expected as we didn't change the perturbation parameter.

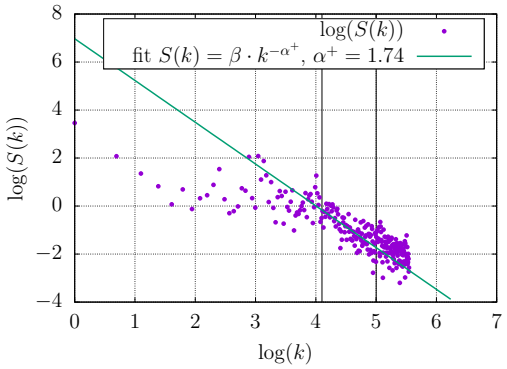

(a) $|\psi^+\rangle$, $\xi = 0.2$

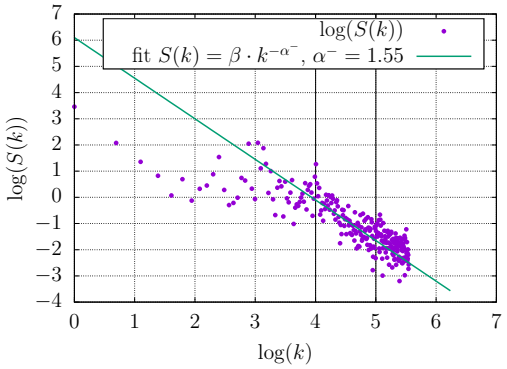

(b) $|\psi^-\rangle$, $\xi = 0.2$

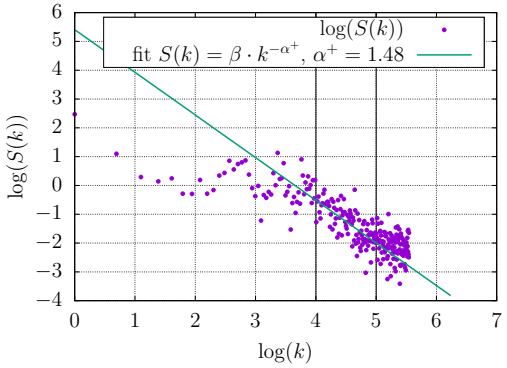

(c) $|\psi^+\rangle$, $\xi = 0.4$

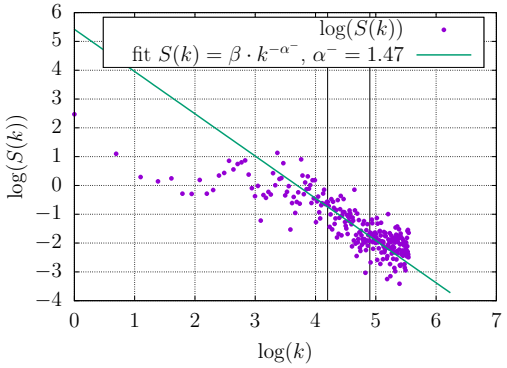

(d) $|\psi^-\rangle$, $\xi = 0.4$

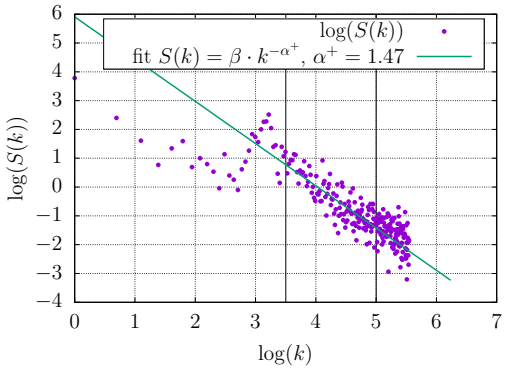

(e) $|\psi^+\rangle$, $\xi = 0.6$

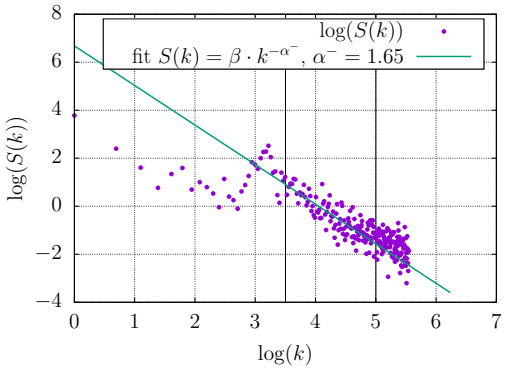

(f) $|\psi^-\rangle$, $\xi = 0.6$

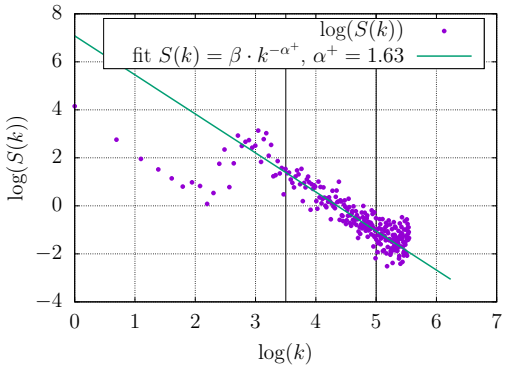

(g) $|\psi^+\rangle$, $\xi = 0.8$

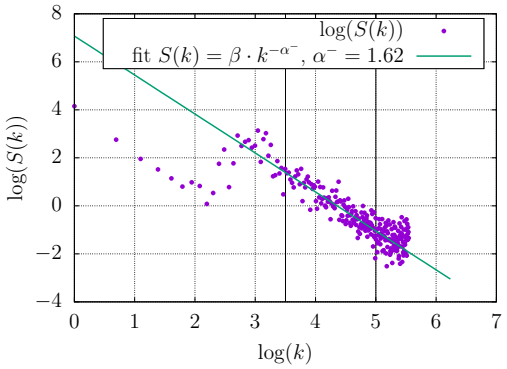

(h) $|\psi^-\rangle$, $\xi = 0.8$

Figure 4.5: Power spectra of the vibron model for $N = 120$, dim $= 7\,381$, $c = 0.4$ and ξ from 0.2 to 0.8. Vertical lines indicate fitting range.

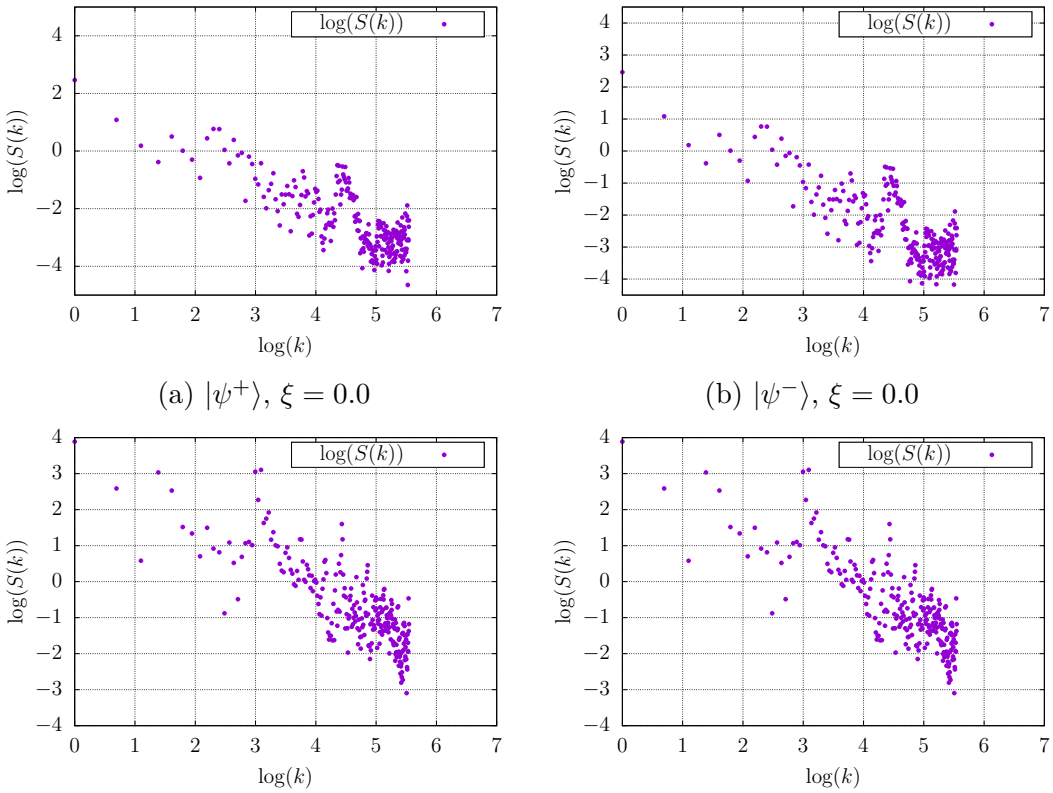

(a) $|\psi^+\rangle$, $\xi = 0.0$ (b) $|\psi^-\rangle$, $\xi = 0.0$

(c) $|\psi^+\rangle$, $\xi = 1.0$ (d) $|\psi^-\rangle$, $\xi = 1.0$

Figure 4.6: Power spectra of the vibron model for $N = 120$, dim $= 7\,381$, $c = 0.4$ and limiting $\xi = 0$ and $\xi = 1$. Vertical lines indicate fitting range.

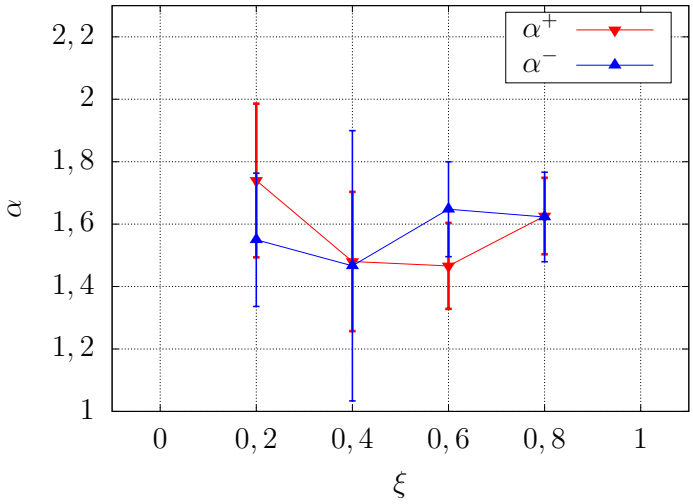

Figure 4.7: The dependence of α on ξ for $c = 0.4$. Points were joined with lines for greater legibility.

4.4 Chaoticity at different energies

In the case of classical chaos, chaoticity depends on the energy of the system. We expect the system to be less chaotic for both very low energies and very high energies. Take for example the well-known classical chaotic system of a double

pendulum. If we perturb it slightly from its rest position, its movement is not as erratic; if we push it strongly, it starts spinning around in a more regular manner. Such behaviour has been shown to be present in the classical limit of the vibron system [10, figures 2.26 and 2.27], we shall now examine this behaviour in the quantum case.

We take $\xi = 0.5$ and $c = 0.4$ as an example of a chaotic configuration. Then we take Hamiltonians for N from 120 to 130. After that we take 512 (after cutting) energy states from each system that are either at the lower, higher or middle position in the spectrum. Next we examine them as if they were ensembles taken from the same system. This approach might seem unphysical, but we consider $N \approx 125$ to already near enough the classical limit $N \to \infty$, so the energy samples for different N should exhibit similar spectral properties.

The exact procedure of our analysis is as follows:

Step 1: We choose a range of values for N, in this case $N \in [120, 130]$.

Step 2: We calculate energy spectra for each N and split the energies into ones belonging to subspace $\{|\psi^+\rangle\}$ and $\{|\psi^-\rangle\}$ as outlined in section 4.2.

Step 3: We choose `window`$= 512$. For each N we

(a) cut the lowest 500 eigenvalues and take the next `window` lowest energies. We save all chosen energies into an array `LOW[]`.

(b) cut the highest 500 eigenvalues and take the next `window` highest energies. We save all chosen energies into an array `HGH[]`.

(c) take the `window` middle energies (i. e. energies from position $i = \dim/2 - $`window`$/2$ to $i = \dim/2 + $`window`$/2$). We save all chosen energies into an array `MID[]`.

Step 4: We analyse the energies in arrays `LOW[]`, `MID[]` and `HGH[]` as we did in section 4.1.

The difference between the analysis in this section and in section 4.2 is shown in fig. 4.9. In principle, it was not necessary choose our energy ranges so coarsely (picking low, medium and high energies) we could have chosen energy ranges in a more granular fashion—for instance 512 energies starting at the n-th level of the spectrum for some n. It would, however, be more difficult to interpret the results and our goal was to provide only a qualitative overview.

The resulting graphs are shown in fig. 4.8. A summary of different coeffiecients α is presented in fig. 4.10.

We see that the chaoticity is lower for lower energies and for the rest of the energies it is approximately the same. Energies at both ends of the spectrum had greater errors in $\alpha^{\pm}$. This could have been caused by the polynomial fit of $\overline{\mathcal{N}}(E)$, which we tried to mitigate by cutting. Again, values for $|\psi^+\rangle$ and $|\psi^-\rangle$ are within error bar range, which should be the case as was explained in section 4.2.

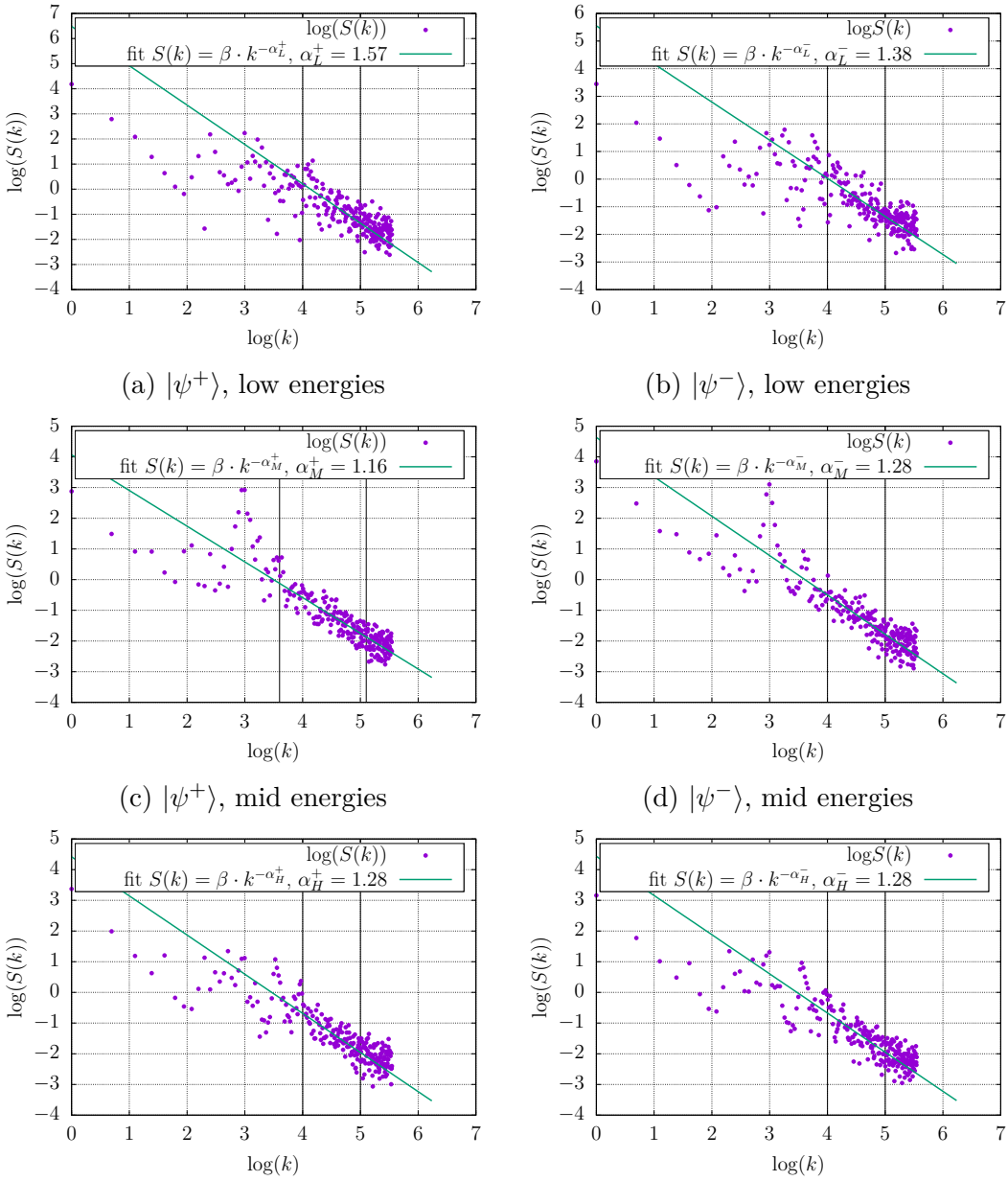

Figure 4.8: Power spectra of vibron models for different energies. N taken from 120 to 130, (dim = 7 381 to 8 646), $\xi = 0.5$ and $c = 0.4$. Eigenlevels from the bottom of the spectrum (L), from the middle of the spectrum (M) and from the top of the spectrum (T) are considered. Vertical lines indicate fitting range.

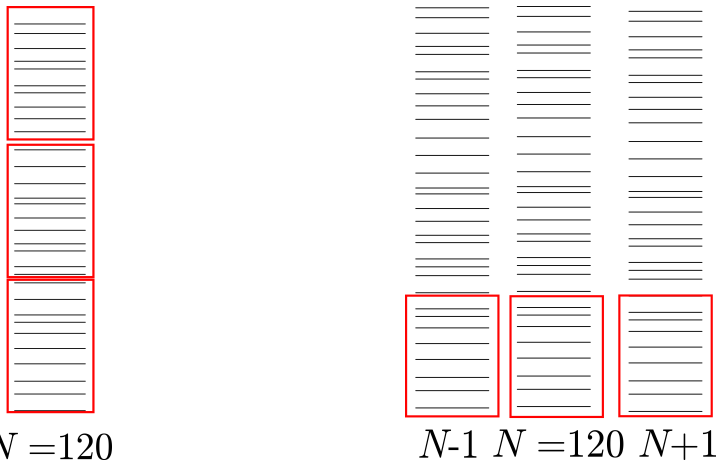

(a) Analysis for different c—one particular value of c

(b) Analysis for different energies—low energies taken

Figure 4.9: The different energies chosen for analysis in sec. 4.1 and 4.4. This image is only illustrative—the actual energy spectra are not shown.

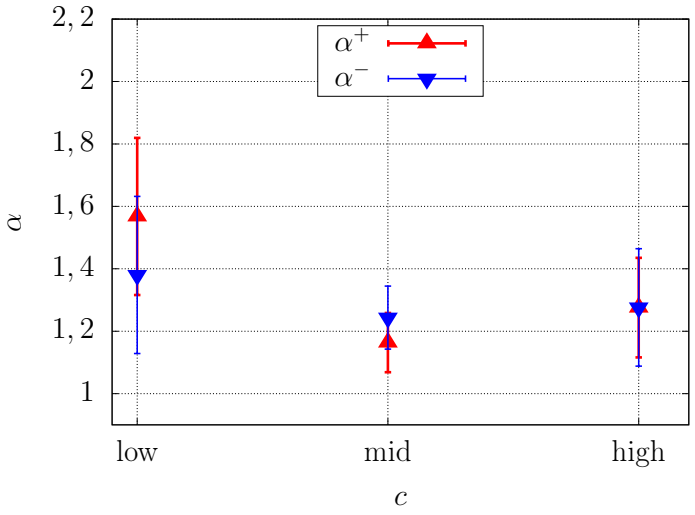

Figure 4.10: Different values of $\alpha^{\pm}$ for low, middle and high energies.

4.5 Efficacy of $1/f$ noise analysis

With the exception of the almost-degenerate cases of $\xi = 0$ and $\xi = 1$, we have observed the predicted $1/f$ noise in all samples. We've been able to determine the α coefficient with varying degrees of accuracy. Errors ranged from ± 0.05 to ± 0.4 in an extreme case; en error around ± 0.1 was the most common.

We don't know how the accuracy of the analysis depends on the value of `window`. A lower `window` means fewer included correlations but also a larger sample size we are working with, which could improve convergence of the observed data. A comparison of different values of `window` is yet to be done.

A persistent problem of this analysis lies in the need of determining fitting boundaries $k_{\min}$ and $k_{\max}$ manually. Firstly, this adds another source of error to the analysis that we cannot easily remove. Secondly, it prevents the process of finding α from being automated. In the present state, we are forced to save

eigenvalues into the memory, test the fitting range and verify whether all is correct. This takes up disk space and also costs time. Due to this, we cannot for instance create a program to automatically map the chaoticity of a given set of parameters. Perhaps the values of $k_{\min}$ and $k_{\max}$ could be estimated by fitting the data with a spline and analysing its derivative, we are not sure if such a procedure would yield consistent results though.

Yet, our analysis also has some benefits. Because $1/f$ noise has links to various other natural phenomena as was described in chapter 2, we gain a greater insight into the meaning of the chaos indicator α and subsequently into the meaning of quantum chaos in general. Albeit with some errors, we have observed $1/f^{\alpha}$ noise which could be interpreted as a measure of chaoticity—we have observed some agreement with the classical case in [10]. Another advantage is that $1/f$ noise contains information about long-range correlations, which sets it apart from other quantum indicators such as the nearest-neighbour spacing distribution described in [22].

Our analysis could be improved to yield more convincing results. This could be done by choosing a larger N. A greater dimension would result in a greater spectral density and thus spectral characteristics would become more apparent. A problem of this approach is the need of diagonalisation of a matrix of order $\dim \approx N^2$. It is widely recognised that the time complexity of a diagonalisation is about $O(\dim^3)$ [28], so this makes increasing the amount of eigenvalues troublesome.

A possible way of reducing the time complexity was outlined in section 4.4, where we experimented with analysing eigenvalues coming from Hamiltonians with similar N as a part of one ensemble. This approach would in theory reduce the complexity of adding new eigenvalues to only $O(\dim)$, but it wouldn't be equivalent to choosing a higher N. Thanks to the Bohigas conjecture, systems with different N should have a similar spectral statistic. But analysing more similar matrices merely improves our sample size. Choosing higher N does this, but also gets closer to the classical limit, which also improves the data.

Conclusion

In this work we have studied quantum chaos in a simple model of molecular vibrations (or a Bose-Einstein condensate). We used the algebraic vibron model presented in [9] and perturbed it to make it more chaotic. The method of determining the chaoticity of the model was the $1/f$ noise analysis presented in [3]. The aim of this work is firstly to map the chaoticity of our system for different parameters and compare it to the classical limit discussed in [10]. As the $1/f$ noise analysis in quantum mechanics is relatively new, the second aim of this work is to determine, how efficient it is in determining the chaoticity of a given system.

During our analysis, we noticed a non-trivial Z_2 (mirror) symmetry. We thus split the spectrum of our Hamiltonian into two subspaces and analysed each one separately to get rid of non-physical correlations.

Nevertheless, we didn't observe the predicted $1/f^2$ noise in an integrable variant of our system. We tried to explain this incongruency by some other correlations we were not aware of, but this explanation needs further testing. For a perturbed system, we observed a more chaotic behaviour as was expected: a partial agreement with the classical limit of our system [10] was recognised. We also measured a system's chaoticity for different energies and observed increased chaoticity for middle and high energies.

Our analysis had relatively high errors, but we suggested ways of improving its accuracy—choosing higher dimension of the observed system, utilising several similar systems or changing the length of the analysed time series. A complex problem we encountered was consistently determining the range of data, where our theory can be applied. This problem makes it difficult to conduct the $1/f$ analysis on a large sample of matrices.

Bibliography

[1] Zdeněk Neubauer. *Golem a další příběhy o kabale, symbolech a podivuhodných setkáních*. Malvern, 2007.

[2] Michael Berry. Quantum chaology, not quantum chaos. *Physica Scripta*, 40:335–336, 1989.

[3] A. Relaño, J. M. G. Gómez, R. A. Molina, J. Retamosa, and E. Faleiro. Quantum chaos and $1/f$ noise. *Phys. Rev. Lett.*, 89:244102, Nov 2002.

[4] J. M. G. Gómez, A. Relaño, J. Retamosa, E. Faleiro, L. Salasnich, M. Vraničar, and M. Robnik. $1/f^{\alpha}$ noise in spectral fluctuations of quantum systems. *Phys. Rev. Lett.*, 94:084101, Mar 2005.

[5] M. Mallon D. Gilden, T. Thornton. $1/f$ noise in human cognition. *Science*, 267:1837–1839, 1995.

[6] Richard F. Voss. Random fractals: Self-affinity in noise, music, mountains, and clouds. *Physica D: Nonlinear Phenomena*, 38:362–371, 1989.

[7] Per Bak, Chao Tang, and Kurt Wiesenfeld. Self-organized criticality: An explanation of $1/f$ noise. phys. rev. lett. 59, 381-384. *Physical Review Letters*, 59:381–384, 08 1987.

[8] Per Bak, Chao Tang, and Kurt Wiesenfeld. Self-organized criticality. *Phys. Rev. A*, 38:364–374, Jul 1988.

[9] F. Iachello and S. Oss. Algebraic approach to molecular spectra: Two-dimensional problems. *The Journal of Chemical Physics*, 104(18):6956–6963, 1996.

[10] Jakub Novotný. *Řád a chaos v jednoduchém modelu molekulárních vibrací*. Charles University, 2004.

[11] Lifschitz Landau. *Mechanics*, volume vol 1. 3 edition.

[12] Pavel Cejnar. *A condensed course of quantum mechanics*. Karolinum Press, 2013.

[13] Pavel Stránský, Petr Hruška, and Pavel Cejnar. Quantum chaos in the nuclear collective model. ii. peres lattices. *Phys. Rev. E*, 79:066201, Jun 2009.

[14] H. Wintgen, D.; Friedrich. Regularity and irregularity in spectra of the magnetized hydrogen atom. *Physical Review Letters*, 57:571–574, 1986.

[15] M. Sieber; F. Steiner. Quantum chaos in the hyperbola billiard. *Physics Letters A*, 148:415–420, 1990.

[16] O. Bohigas, M. J. Giannoni, and C. Schmit. Characterization of chaotic quantum spectra and universality of level fluctuation laws. *Phys. Rev. Lett.*, 52:1–4, Jan 1984.

[17] M.L. Mehta. *Random Matrices*. ISSN. Elsevier Science, 2004.

[18] Ángel L. Corps and Armando Relaño. Long-range level correlations in quantum systems with finite hilbert space dimension. *Phys. Rev. E*, 103:012208, Jan 2021.

[19] Fritz Haake. *Quantum Signatures of Chaos*. Springer Berlin Heidelberg, 2010.

[20] E. Faleiro, J. M. G. Gómez, R. A. Molina, L. Muñoz, A. Relaño, and J. Retamosa. Theoretical derivation of $1/f$ noise in quantum chaos. *Phys. Rev. Lett.*, 93:244101, Dec 2004.

[21] M. Tabor M. V. Berry. Level clustering in the regular spectrum. *Proceedings Mathematical Physical & Engineering Sciences*, 356:375–394, 1977.

[22] T. A. Brody. A statistical measure for the repulsion of energy levels. *Lettere Al Nuovo Cimento Series 2*, 7:482–484, 1973.

[23] Yu Zhang and Wenting Dong. Two-particle transfer intensities in excited-state quantum phase transition. *AIP Conference Proceedings*, 2150(1):040007, 2019.

[24] Michael Rautenberg and Martin Gärttner. Classical and quantum chaos in a three-mode bosonic system. *Phys. Rev. A*, 101:053604, May 2020.

[25] F. iachello, r.d. levine: Algebraic theory of molecules, oxford university press, new york, oxford, isbn 0-19-508091-2, 1995. *Berichte der Bunsengesellschaft für physikalische Chemie*, 99(4):694–694, 1995.

[26] F. Iachello, F. Pérez-Bernal, and P.H. Vaccaro. A novel algebraic scheme for describing nonrigid molecules. *Chemical Physics Letters*, 375(3):309–320, 2003.

[27] Keith Benedict. Understanding quantum phase transitions, edited by lincoln carr. *Contemporary Physics - CONTEMP PHYS*, 53:1–2, 07 2012.

[28] Victor Y. Pan and Zhao Q. Chen. The complexity of the matrix eigenproblem. In *Proceedings of the Thirty-First Annual ACM Symposium on Theory of Computing*, STOC '99, page 507–516, New York, NY, USA, 1999. Association for Computing Machinery.

List of Figures

List of Tables